Applied Catalysis B: Environmental 96 (2010) 208–217

Contents lists available at ScienceDirect

Applied Catalysis B: Environmental

journal homepage: www.elsevier.com/locate/apcatb

# Photo-Fenton-like treatment of the commercially important H-acid: Process optimization by factorial design and effects of photocatalytic treatment on activated sludge inhibition

Idil Arslan-Alaton*, Nuray Ayten, Tugba Olmez-Hanci

*Istanbul Technical University, Faculty of Civil Engineering, Department of Environmental Engineering, 34469 Maslak, Istanbul, Turkey*

ARTICLE INFO

*Article history:*
Received 5 January 2010
Received in revised form 11 February 2010
Accepted 13 February 2010
Available online 23 February 2010

*Keywords:*
H-acid
Response surface methodology
Central composite design
Photo-Fenton-like oxidation process
Activated sludge inhibition

ABSTRACT

H-acid is a biologically inert, photochemically stable napthalene sulphonate derivative (1-amino-8-hydroxynaphthalene-3,6-disulphonic acid) being frequently produced as an essential raw material of many commercially available textile azo dyes. Treatability reports dealing with the advanced chemical oxidation of H-acid are limited to a few case studies that do not provide a deep insight into single as well as combinative effects of the main process variables influencing the treatment performance. In the present study, the degradation of aqueous H-acid and its organic carbon (COD, TOC) content with the Photo-Fenton-like advanced oxidation process was optimized in terms of selected major process variables (ferric iron concentration, hydrogen peroxide concentration, initial COD value and reaction time) by employing response surface methodology and central composite design. For this purpose, two main targets were set in the optimization approach, namely (i) the achievement of complete/highest possible oxidation (mineralization) and a (ii) partial oxidation option under relatively mild reaction conditions. The photocatalytic treatment performance was examined by the analysis of the process outputs H-acid, COD and TOC removals. Statistical evaluation of the established polynomial regression models as well as validation experiments run under locally (initial COD-based) optimized reaction conditions to test the reliability of the obtained models revealed that Photo-Fenton-like oxidation of aqueous H-acid is highly efficient and the proposed reaction model successfully predicts organic carbon abatement rates for both treatment targets. From the empirical regression models derived for organic carbon removal it was also evident that the photocatalytic treatment system was mainly affected by the initial COD content (negative effect) closely followed by the parameter initial hydrogen peroxide concentration (positive effect). Activated sludge inhibition experiments conducted with heterotrophic biomass indicated that during the application of Photo-Fenton treatment under optimized reaction conditions, no toxic oxidation products were formed.



## 1. Introduction

Naphthalene sulphonates are used as precursors for sulphonated azo dyes, wetting agents, leveling agents, dispersants, optical brighteners, pesticides, ion exchange resins, pharmaceuticals and concrete plasticizers, etc. at considerably high amounts [1,2]. For instance, the annual world production of azo dyes from H-acid is estimated to be around one million tons [3]. Recently, the production of commercially important naphthalene sulphonates such as H-acid has been limited since their discharge into receiving water bodies has led to serious environmental pollution problems in the main providing countries [4]. After production and use in different industrial processes, naphthalene sulphonates are easily discarded into the aquatic environment and do not significantly sorb on biosludge or sediments due to their hydrophilic, polar nature [5]. It has been deduced that their concentration in European river and surface waters is detectable at ng/L to μg/L levels, whereas their concentration is relatively lower in U.S. water bodies [2]. However, their actual concentrations in industrial wastewater treatment plants are much higher, i.e. in the μg/L to mg/L range [2]. Although naphthalene sulphonates themselves impart a low acute biotoxicity and have neither mutagenic nor carcinogenic effects, due to the deactivating nature of their sulphonated functional groupings (R-$SO_3$H), naphthalene sulphonates have an extremely low reactivity against electrophilic addition reactions including microbial degradation [6]. As a consequence, alternative and more efficient treatment process have to be developed for the degradation of naphthalene sulphonates.

* Corresponding author. Tel.: +90 212 285 37 86; fax: +90 212 285 65 45.
*E-mail address:* arslanid@itu.edu.tr (I. Arslan-Alaton).

0926-3373/$ – see front matter © 2010 Elsevier B.V. All rights reserved.
doi:10.1016/j.apcatb.2010.02.023

Ozonation and advanced oxidation processes (AOPs) have recently emerged as an important class of technologies applied for the destructive treatment of a wide range of recalcitrant and/or toxic pollutants found in water and wastewater [7–9]. These treatment processes can either completely eliminate these pollutants through mineralization to carbon dioxide, water and mineral salts, or partially convert them to degradation products that are less harmful to human health and the aquatic environment, or more prone to biodegradation. Chemical oxidation processes dedicated to the treatment of naphthalene sulphonates are ozonation at varying pHs and ozone doses [10–12], $H_2O_2$/UV [13], Photo-Fenton and electro-Fenton [14,15] processes, electrochemical [14,16] and photoelectrochemical [16–18] treatment, and heterogeneous photocatalysis using titanium dioxide [19,20]. Among these AOPs, iron-based advanced oxidation processes have gained more attention and popularity due to possibility of using near-UV or even solar radiation as the light source, their relatively high efficiency, fast degradation kinetics, relative low costs and high abundance of employed chemicals (Fe, $H_2O_2$). In the Fenton's reaction, hydroxyl radicals ($HO^\bullet$) are generated by the catalytic decomposition of $H_2O_2$ in acidic medium (pHs 2–5) [21]. Photo-Fenton oxidation is the photocatalytically enhanced version of the Fenton process; in the Photo-Fenton process; UV light irradiation causes an increase in the $HO^\bullet$ formation rate and efficiency via photoreduction of $Fe^{3+}$ to $Fe^{2+}$, thus continuing the redox cycle as long as $H_2O_2$ is available [22–25]

$$Fe(III)OH^{2+} + h\upsilon \rightarrow Fe^{2+} + HO^\bullet \qquad k_1 = 0.0012\,s^{-1} \tag{1}$$

The quantum yield of the above process is pH and wavelength-dependent. As compared with the Photo-Fenton process, Photo-Fenton-like ($Fe^{3+}/H_2O_2$/UV) treatment has been explored in fewer studies, although its efficiency is thought to be practically identical to that of the Photo-Fenton process due to the fact that the rate-limiting step of Fe-based advanced oxidation processes is the relatively slow catalytic reaction between ferric ion and hydrogen peroxide [22,24,26]

$$Fe^{3+} + H_2O_2 \leftrightarrow Fe(OOH)^{2+} + H^+ \qquad k_2 = 3.1 \times 10^{-3} \tag{2}$$

$$Fe(OOH)^{2+} \rightarrow HO_2^\bullet + Fe^{2+} \qquad k_3 = 2.7 \times 10^{-3}\,s^{-1} \tag{3}$$

Considering that naphthalene sulphonates are very difficult-to-oxidize compounds and our previous work investigating $H_2O_2$/UV-C treatment of commercially important naphthalene sulphonates (H-, K-, J-acid and the aryl sulphonate formulation Para base) resulted in very low oxidation efficiencies and slow degradation kinetics [13], UV light-assisted Fenton-like oxidation appears to be a more suitable option for the treatment of naphthalene sulphonates. However, it should be considered that advanced oxidation may result in the formation of more inert and/or toxic degradation products, since free radical chain reaction-based treatment methods are difficult to control thus requiring the toxicity assessment of the formed advanced oxidation intermediates [27–29].

Several process variables such as pH, treatment time, initial iron catalyst, hydrogen peroxide and pollutant concentrations affect the Photo-Fenton oxidation efficiency and may interact with each other [23,24,26]. In this manner, process optimization cannot be straightforward. Although in most related case studied a single-factor-at-a-time approach (varying one process variable thereby keeping the others constant) was used for the optimization of AOP conditions, it is already known that this approach is very time consuming, and more importantly, does not consider that for some parameters not only individual, but also combinative impacts are involved. In fact, a better optimization approach is to employ multivariate analysis to optimize and model the degradation of a refractory index pollutant by Photo-Fenton-like oxidation. Response surface methodology (RSM) as a powerful mathematical and statistical design tool that can be used to evaluate and optimize the performance of complex systems by considering the relative significance of several affecting factors even in the presence of complicated, multi-dimensional interactions [30].

Several studies are available in the scientific literature reporting the combinative effects of process variables affecting the Photo-Fenton or Fenton processes and observed similar relationships for different industrial effluents and single model pollutants [31–34]. However, until now, statistical design tools have not been used to model and optimize AOP (i) for different initial pollutant concentrations (organic pollution loads) and (ii) by setting multiple targets to achieve treatment efficiencies at different levels depending upon legislative or other requirements. Addressing this issue is of utmost importance, since AOP are quite energy-intense processes and only applicable if very specific economically and technically feasible treatment goals are set. Considering all the above indicated facts, Photo-Fenton-like oxidation of a naphthalene sulphonic acid formulation being frequently used for the synthesis of azo dyes, e.g. H-acid, was investigated and optimized via central composite design (CCD). For that purpose, a series of iterative Photo-Fenton-like experiments were firstly conducted with aqueous H-acid solution to identify the experimental design range. Treatment performance was assessed in terms of H-acid, COD and TOC removal efficiencies. Thereafter, Photo-Fenton-like oxidation of H-acid was modeled and optimized in terms of organic carbon removals at different initial CODs being typical for textile dye production effluents by setting two different targets (complete-maximum and partial oxidation). The established polynomial regression models were validated by running separate experiments under Photo-Fenton-like oxidation conditions being previously optimized for different initial CODs. In the last stage of the study, separate experiments were run at the same local optima to examine the inhibitory effect of Photo-Fenton-like treatment of aqueous H-acid on the oxygen uptake rate of activated sludge microorganisms (heterotrophic biomass).

## 2. Experimental

### 2.1. Materials

The commercial-grade H-acid ($C_{10}O_7H_9NS_2$; MW: 319; 85%) was supplied by a local dye manufacturing plant and used as received without any further purification. H-acid was weighted and dissolved in distilled water to attain required COD values used in the study. 35% (w/w) $H_2O_2$ (Fluka, USA) was used as received without any dilution. Residual $H_2O_2$ was destroyed with enzyme catalase derived from *Micrococcus lysodeikticus* (100,181 U $mL^{-1}$, Fluka, USA). The ferric iron catalyst source was prepared for daily use by dissolving $Fe(NO_3)_3{\cdot}9H_2O$ (Fluka, USA) in distilled water to obtain a 10% (w/v) stock solution. Several concentrations of $HNO_3$ (Merck, Germany) and NaOH (Merck, Germany) solutions were used for pH adjustment. HPLC-grade acetonitrile was obtained from Merck (Germany). All other reagents were analytical grade and used without purification.

### 2.2. Experimental procedure for Photo-Fenton-like oxidation

All experiments were conducted at room temperature in a cylindrical Pyrex glass reaction vessel with a capacity of 100 mL. A 150 W black light bulb lamp, emitting radiation between 310 and 390 nm and having a maximum emission band at 360–365 nm was used as the UV-A light source. The photoreactor was located inside a box (dimensions = 60 cm × 40 cm × 55 cm) with its three inner sides covered by mirrors enabling homogenous and efficient UV-A

**Table 1**
Definition of the experimental design matrix.

| Experiment no. | $X_1$-$t_r$ (min) | $X_2$-$COD_o$ (mg/L) | $X_3$-$H_2O_2$ (mM) | $X_4$-$Fe^{3+}$ (mM) |
|---|---|---|---|---|
| 1 | 12 (−1) | 600 (1) | 20 (−1) | 2.0 (1) |
| 2 | 6 (−2) | 450 (0) | 30 (0) | 1.5 (0) |
| 3 | 18 (0) | 450 (0) | 30 (0) | 0.5 (−2) |
| 4 | 12 (−1) | 600 (1) | 40 (1) | 1.0 (−1) |
| 5 | 18 (0) | 450 (0) | 30 (0) | 2.5 (2) |
| 6 | 24 (1) | 300 (−1) | 40 (1) | 2.0 (1) |
| 7 | 18 (0) | 150 (−2) | 30 (0) | 1.5 (0) |
| 8 | 24 (1) | 600 (1) | 40 (1) | 2.0 (1) |
| 9 | 24 (1) | 300 (−1) | 20 (−1) | 1.0 (−1) |
| 10 | 12 (−1) | 600 (1) | 20 (−1) | 1.0 (−1) |
| 11 | 30 (2) | 450 (0) | 30 (−1) | 1.5 (0) |
| 12 | 12 (−1) | 600 (1) | 40 (1) | 2.0 (1) |
| 13 | 18 (0) | 450 (0) | 30 (0) | 1.5 (0) |
| 14 | 18 (0) | 450 (0) | 50 (2) | 1.5 (0) |
| 15 | 12 (−1) | 300 (−1) | 40 (1) | 1.0 (−1) |
| 16 | 12 (−1) | 300 (−1) | 20 (−1) | 1.0 (−1) |
| 17 | 24 (1) | 600 (1) | 20 (−1) | 2.0 (1) |
| 18 | 18 (0) | 450 (0) | 10 (−2) | 1.5 (0) |
| 19 | 18 (0) | 450 (0) | 30 (0) | 1.5 (0) |
| 20 | 24 (1) | 600 (1) | 20 (−1) | 1.0 (−1) |
| 21 | 12 (−1) | 300 (−1) | 40 (1) | 2.0 (1) |
| 22 | 24 (1) | 600 (1) | 40 (1) | 1.0 (−1) |
| 23 | 24 (1) | 300 (−1) | 40 (1) | 1.0 (−1) |
| 24 | 18 (0) | 750 (2) | 30 (0) | 1.5 (0) |
| 25 | 24 (1) | 300 (−1) | 20 (−1) | 2.0 (1) |
| 26 | 12 (−1) | 300 (−1) | 20 (−1) | 2. 0 (1) |

light distribution. The intensity of the incident light flux inside the photoreactor was measured via ferrioxalate actinometry [35] and determined as $2.6 \times 10^{-5}$ einstein/min. The reaction solution was continuously stirred with a magnetic bar to ensure sufficient oxygen supply and mixing. The experimental procedure of a typical photo-Fenton-like experimental run is described elsewhere [36]. Samples were taken at regular time intervals for HPLC, COD, TOC, residual $H_2O_2$ and pH analyses.

### 2.3. Establishment of the experimental design matrix using factorial design

In order to explore the effect of independent process variables on the responses within the range of investigation, a CCD with four independent (process) variables ($X_1$, reaction time (min); $X_2$, initial COD value (mg/L); $X_3$, $H_2O_2$ concentration (mM); $X_4$, $Fe^{3+}$ concentration (mM)) at five levels was performed. The independent variables and their ranges were chosen based on preliminary experimental results. The whole design consisted of 26 experimental runs carried out in random order, which included 16 factorial points, 2 centre and 8 axial points. Table 1 shows the coded (in brackets) and actual values of the independent variables at which the experiments were conducted to estimate the response variables COD removal (% $Y_1$) and TOC removal (% $Y_2$). Each response was used to develop an empirical model which correlated the responses to the four process variables. The empirical regression model is presented in Eq. (4) [30]

$$Y = b_0 + \Sigma b_i X_i + \Sigma b_{ii} X_i^2 + \Sigma b_{ij} X_i X_j \quad (4)$$

In the above equation, $Y$ represents the predicted responses, $X_i$s are the independent process variables, $b_o$ is the constant coefficient and $b_i$, $b_{ii}$ and $b_{ij}$ are the interaction coefficients. The fitted polynomial equation was expressed in the form of surface and contour plots in order to visualize the relationship between the responses and experimental levels of each process variables and to deduce the optimum conditions [30]. Analysis of variance (ANOVA) for the model was also carried out to deduce its statistical significance and reliability. The significances of all model terms in the polynomial equation were judged statistically by computing the $F$-value (Fisher variation ratio) at a probability value (Prob > $F$) of 0.050. The regression coefficients were then used to conduct statistical calculations and generate dimensional/contour maps from the regression models. The ANOVA and response surfaces were performed using the Design Expert Software (Version 7.1.5) from Stat-Ease Inc., USA. The Photo-Fenton-like process conditions being optimized for organic carbon removals at different initial CODs at two different targets (complete-maximum and partial oxidation) were estimated using the software's numerical and graphical optimization tools. It should be emphasized herein that although being measured during the photocatalytic experiments via HPLC, the parent compound (surfactant) was not considered as the main process response, since its abatement was very fast and completed within minutes during $H_2O_2$/UV-C oxidation (data not shown).

### 2.4. Analytical procedures

During the photocatalytic experiments, parent compound (H-acid), COD and TOC parameters were measured at regular treatment time intervals. All analytical measurements were performed after filtration of the treated samples though 0.45 μm cellulose acetate membrane filters (Millipore) in order to remove the ferric hydroxide precipitate. The amount of H-acid was monitored via HPLC (Agilent 1100 Series, USA) equipped with a Diode-Array Detector (DAD) detector (G1315A, Agilent Series) and an Atlantis C18 (3.9 mm × 150 mm, 5 μm, Waters) column, at 358 nm. Acetonitrile–water solution (60:40, v/v) was employed as the mobile phase at a flow rate of 1 mL/min. The quantification limit for H-acid detection was found as 5 mg/L. COD of the samples was determined by the closed reflux titrimetric method according to ISO 6060 [37]. Prior the all COD measurements residual (unreacted) $H_2O_2$ was destroyed with enzyme catalase to quench the photocatalytic reaction and prevent positive interferences with the COD measurements. An organic carbon analyzer (Shimadzu $V_{CPN}$, Japan) was used to determine the TOC content of reaction samples by the combustion-infrared method. TOC was estimated by the difference between the total carbon (TC) and the inorganic carbon (IC) in the samples. $H_2O_2$ was measured by the molybdate catalyzed, standard iodometric titration method [38]. Analytical measurements were done in triplicate and the standard deviations for the measurements were found to be within the ranges given by the methods' procedures. The pH was measured with a Thermo Orion model 720 pH-meter at any stage of the experiments.

### 2.5. Activated sludge inhibition experiments

The procedure of the activated sludge inhibition experiments was based on the test protocol previously described in ISO 8192 [39]. The activated sludge used as the heterotrophic biomass was obtained from a municipal tertiary wastewater treatment located in Istanbul and daily fed with synthetic sewage in accordance with the same test protocol [31–34]. The activated sludge inhibition experiments were conducted with untreated and photocatalytically treated aqueous H-acid solutions (samples being exposed to Photo-Fenton-like oxidation at different time intervals under optimized reaction conditions) similar to our former work [40,41]. In the present study, the MLVSS concentration used in the activated sludge inhibition experiments was adjusted to 1500 mg/L, respectively, to obtain appropriate oxygen uptake rates (OUR, in mg/(L h)) of around 100 ± 5 mg/(L h). Any unreacted $H_2O_2$ remaining in the Photo-Fenton-like treated aqueous H-acid was destroyed with catalase enzyme and the pH of the solutions was adjusted to 7.0 ± 0.2 before conducting the experiments in order to eliminate potential inhibitory effects of $H_2O_2$ and pH, respectively. The experiments were conducted for up to 180 min. The percent inhibitory effect on OUR ($I_{OUR}$, in %) of the test samples relative to blank con-

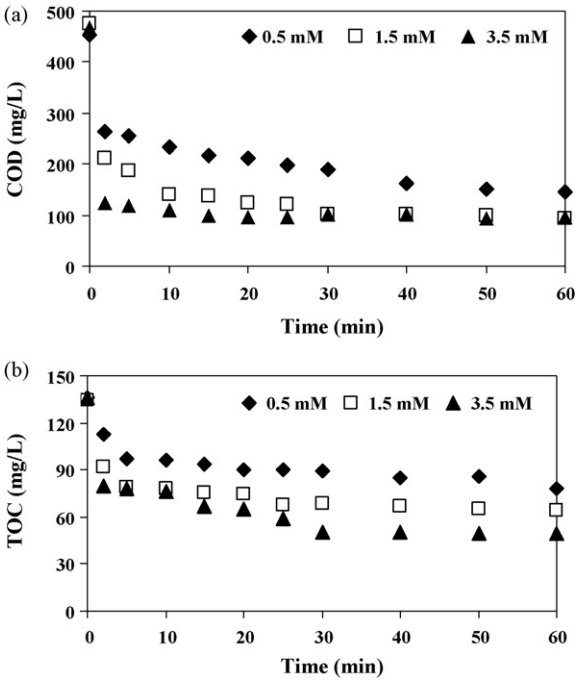


**Fig. 1.** Time-dependent changes in COD (a) and TOC (b) parameters at three different $Fe^{3+}$ concentrations. Experimental conditions: $COD_o$ = 450 mg/L; applied $H_2O_2$ = 30 mM; $pH_o$ = 3.0.

trols (containing synthetic sewage only with a COD of 480 mg/L) for different dilutions of the test samples with synthetic sewage, was calculated by using the following formula [39]

$$I_{OUR}(\%) = \frac{OUR_S - OUR_B}{OUR_B} \times 100 \quad (5)$$

where $OUR_S$ is the OUR in the reaction samples and $OUR_B$ stands for the OUR in the sample blank.

## 3. Results and discussion

### 3.1. Iterative Photo-Fenton-like oxidation experiments

In order to select the most appropriate working ranges for the factorial design of Photo-Fenton-like treatment of aqueous H-acid solution, three sets of Photo-Fenton-like experiments were conducted at varying pHs (at pH 2, 3, 4 and 5; thereby keeping $H_2O_2$ and $Fe^{3+}$ concentrations constant at 35 and 1.5 mM, respectively), $H_2O_2$ concentrations (15, 20, 30 and 35 mM; thereby keeping the pH and $Fe^{3+}$ concentration constant at 3 and 1.5 mM, respectively) and $Fe^{3+}$ concentrations (0.5, 1.5 and 3.5 mM; thereby keeping the pH and $H_2O_2$ concentration constant at 3 and 1.5 mM, respectively). The initial COD of H-acid was 450 mg/L in these experiments, which is an average, typical COD for effluents containing H-acid as the main organic pollutant [42]. The total photocatalytic treatment time was fixed at 60 min due to the fact that iron-based advanced oxidation processes proceed very fast and the most significant removal occurs promptly, within the first 5–15 min of the oxidation reaction. Fig. 1 displays COD (a) and TOC (b) abatement rates obtained during Photo-Fenton-like treatment of aqueous H-acid at 3 different $Fe^{3+}$ concentrations.

From Fig. 1 it is evident that, as expected, COD as well as TOC evolutions are very fast and slow down appreciably after the first 5–10 min of Photo-Fenton-like treatment. Thereafter, depending on the applied $Fe^{3+}$ concentration, photocatalytic H-acid degradation continues until either $H_2O_2$ is practically consumed and/or degradation intermediates more resistant to oxidative attack (i.e. carboxylic acids) build up in the reaction solution [13]. As a consequence of the almost promptly occurring oxidation reaction, no detailed kinetic analysis could be conducted and it was decided to evaluate the initial COD and TOC rates obtained at different initial $Fe^{3+}$ concentrations. In terms of the COD parameter, elevating the photocatalyst from 0.5 to 1.5 mM, increased the initial COD abatement rate considerably from 98 to 132 mg/(L min), and for a further increase to 3.5 mM the initial COD abatement rate was enhanced to 171 mg/(L min) indicating the positive effect of $Fe^{3+}$ on photocatalytic reaction rates. The initial rates calculated for the TOC parameter were 20, 22 and 31 mg/(L min). Hence, it is clear that the accelerating influence was also reflected on TOC abatement kinetics, however, the catalytic effect was more pronounced at the higher $Fe^{3+}$ concentration and the improvement was not so dramatic as for the COD parameter. Almost 95% of the initially present $H_2O_2$ was consumed after 35–40 min leading to the accumulation of $Fe^{2+}$ in the reaction solution; photoreduction of ferri-hydroxo and/or ferri-organo complexes producing $Fe^{2+}$, additional $HO^{\bullet}$ and organic radicals continues the radical chain reactions to a certain extent even in the absence of $H_2O_2$. However, this contribution to the degradation of H-acid and its intermediates is relatively minor as compared with the dark Fenton ($Fe^{2+}/H_2O_2$) reaction being responsible for the main reduction in the organic carbon content of H-acid. The positive effect of increasing $Fe^{3+}$ concentration on both COD and TOC abatement rates and efficiencies is quite obvious from Fig. 1, supporting the fact that $Fe^{3+}$ has an important role in organic carbon abatement. Hence, its concentration has to be definitely considered as a major process independent variable for the factorial design procedure. Increasing the initially introduced $H_2O_2$ concentration from 15 to 20 mM also had a significant influence on COD and TOC removal rates (data not shown); however, an increase of the applied $H_2O_2$ concentration up to 30 and 35 mM did not further enhance treatment efficiencies for an initial H-acid concentration corresponding to 450 mg/L COD. On the other hand, within the investigated pH range (=2–5) that is known to be the effective pH range for Fenton and Photo-Fenton treatment systems, no effect in treatment performance was experimentally observed during Photo-Fenton-like oxidation of aqueous H-acid. This is not surprising since the studied pHs were in the optimum range as mentioned above. The results of the complete set of iterative Photo-Fenton-like oxidation experiments were not presented in detail in this study since they only confirmed previous findings reported in our as well as other related scientific work [43,44]. However, considering the information derived from these preliminary experiments, the number, type and range of process independent variables could be identified for the establishment of the factorial design that was used to model and optimize Photo-Fenton-like treatment of H-acid. For instance, it was decided to conduct the Photo-Fenton-like experiments for the central composite design at pH = 5 rather than pH = 3, that is usually the more typical pH for iron-based advanced oxidation processes, since pH = 5 is closer to neutral, more biocompatible pHs. In addition, several control experiments were conducted in order to elucidate the dominant reaction mechanism taking place during photocatalytic degradation of H-acid. These experimental runs were planned as follows; in the absence of (a) UV-A light (to examine the contribution of the dark Fenton reaction); (b) $Fe^{3+}$ ions (contribution of $H_2O_2$ oxidation and UV-A irradiation) and (c) $H_2O_2$ (contribution of $Fe^{3+}$ photoreduction and coagulation). In summary, obtained experimental findings indicated that the degradation due to cases (b) and (c) was marginal in terms of both COD ($\leq$11%) and TOC ($\leq$8%) removal efficiencies. However, the contribution of the direct Fenton-like oxidation was considerable; 77% and 42% COD and TOC removals were obtained after 30 min Fenton-like treatment (reaction conditions: $COD_o$ = 450 mg/L; $Fe^{3+}$ = 1.5 mM; $H_2O_2$ = 35 mM and $pH_o$ = 5.0). These results were quite similar to the treatment efficiencies achieved under UV-A light irradiation

**Table 2**
Experimental design matrix results for Photo-Fenton-like oxidation of aqueous H-acid solution. For reaction conditions foreseen by the central composite design see Table 1.

| Experiment no. | COD removal Experimental (%) | COD removal Model (%) | TOC removal Experimental (%) | TOC removal Model (%) |
|---|---|---|---|---|
| 1 | 48 ± 5 | 51 | 17 ± 2 | 18 |
| 2 | 65 ± 7 | 69 | 29 ± 3 | 35 |
| 3 | 45 ± 5 | 54 | 19 ± 2 | 23 |
| 4 | 50 ± 5 | 57 | 22 ± 2 | 25 |
| 5 | 76 ± 8 | 74 | 33 ± 3 | 33 |
| 6 | 74 ± 7 | 78 | 45 ± 5 | 49 |
| 7 | 76 ± 8 | 83 | 45 ± 5 | 51 |
| 8 | 77 ± 8 | 83 | 41 ± 4 | 41 |
| 9 | 78 ± 8 | 74 | 38 ± 4 | 37 |
| 10 | 37 ± 4 | 33 | 14 ± 1 | 13 |
| 11 | 78 ± 8 | 81 | 48 ± 5 | 46 |
| 12 | 72 ± 7 | 76 | 35 ± 4 | 34 |
| 13 | 74 ± 7 | 76 | 34 ± 3 | 37 |
| 14 | 77 ± 8 | 71 | 44 ± 4 | 52 |
| 15 | 69 ± 7 | 67 | 44 ± 4 | 39 |
| 16 | 71 ± 7 | 69 | 34 ± 3 | 32 |
| 17 | 52 ± 5 | 55 | 17 ± 2 | 19 |
| 18 | 31 ± 3 | 44 | 7 ± 1 | 8 |
| 19 | 75 ± 8 | 76 | 39 ± 4 | 37 |
| 20 | 42 ± 4 | 43 | 16 ± 2 | 15 |
| 21 | 72 ± 7 | 76 | 44 ± 4 | 44 |
| 22 | 67 ± 7 | 69 | 33 ± 3 | 36 |
| 23 | 75 ± 8 | 76 | 51 ± 5 | 49 |
| 24 | 53 ± 5 | 53 | 21 ± 2 | 18 |
| 25 | 77 ± 8 | 74 | 42 ± 4 | 38 |
| 26 | 77 ± 8 | 75 | 44 ± 4 | 38 |

after 30 min Photo-Fenton-like oxidation (80% COD and 54% TOC removals) under otherwise identical reaction conditions. From the above findings it is evident that the difference in oxidation performance between the dark and UV-A-enhanced processes is more pronounced in terms of the TOC parameter representing the degree of ultimate oxidation; in our previous studies we could demonstrate that Photo-Fenton-like treatment under UV-A irradiation has no additional, positive effect on parent compound (dye, dye precursor) abatement, but results in higher organic carbon removals than those observed in Fenton-like treatment [44]. H-acid itself exhibits a strong absorption band at 358–360 nm coinciding with the dominant emission band of the UV-A light source employed in the present study. The extinction coefficient of H-acid at 365 nm is 6900 $M^{-1}\,cm^{-1}$; hence H-acid at least partially competes with Ferric-hydroxo and ferric-organo complexes for UV-A light absorption. As a consequence, at least within the first stages of the oxidation process, the photoreduction of $Fe^{3+}$ complexes to $Fe^{2+}$ and hence additional $HO^{\bullet}$ formation that is shown in Eq. (1) is partially inhibited. On the other hand, Photo-Fenton-like oxidation intermediates may form complexes with ferric iron that are photochemically active and cause enhanced mineralization in the presence of UV-A light, thus confirming the main role of $HO^{\bullet}$ in TOC removal.

### 3.2. Process design experiments

26 sets of Photo-Fenton-like experiments were carried out as foreseen by the CCD matrix and for each experimental run, percent COD and TOC removal efficiencies were determined (Table 2). The experimental findings obtained under varying reaction conditions were processed by the Design Expert® software of the design module and second order polynomial regression models were established in terms of the selected process independent variables (coded values) to describe percent COD and TOC removal efficiencies as follows

$$\begin{aligned}\text{COD Removal}\,(\%) = {} & 74.16 + 3.01 \times X_1 - 8.21 \times X_2 + 6.86 \times X_3 \\ & + 5.07 \times X_4 + 1.01 \times X_1X_2 + 6.17 \times X_2X_3 \\ & + 0.55 \times X_3X_4 + 2.93 \times X_2X_4 - 1.49 \times X_1X_4 \\ & + 0.81 \times X_1X_3 - 2.03 \times X_2^2 - 3.06 \times X_4^2 \\ & - 4.66 \times X_3^2 - 0.32 \times X_1^2 \end{aligned} \quad (6)$$

$$\begin{aligned}\text{TOC Removal}\,(\%) = {} & 36.59 + 2.79 \times X_1 - 8.14 \times X_2 + 7.09 \times X_3 \\ & + 2.47 \times X_4 + 0.47 \times X_1X_2 + 1.23 \times X_1X_3 \\ & + 1.06 \times X_2X_4 + 2.48 \times X_2X_3 - 0.19 \times X_3X_4 \\ & - 1.31 \times X_1X_4 - 0.48 \times X_2^2 - 2.14 \times X_4^2 - 2.31 \\ & \times X_3^2 + 0.98 \times X_1^2 \end{aligned} \quad (7)$$

For $-2 \le X_i \le 2$.

The effect of each process independent variable can be directly attributed to its coefficient value [30]. As such, more effective factors possess higher absolute values. The parameter's (process independent variable) coefficients as well as its algebric sign are considered to evaluate the relative effect of each variable on the process outputs (in the present case: COD and TOC removals). From the quadratic equation established for percent COD removal efficiency, it can be concluded that the process variable that has the most significant impact on COD removal is the initial COD of aqueous H-acid solution ($COD_o$) and the effect is negative; i.e. increasing the COD content of the reaction solution decreases the photocatalytic oxidation efficiency. The other process variables had all positive influences on COD removal rates; the effect of initially added $H_2O_2$ was followed by the $Fe^{3+}$ concentration, whereas photocatalytic treatment time ($t_r$) had the least effect upon all studied process independent variables. Upon closer inspection of the polynomial regression model obtained for the TOC parameter, it is obvious that again the initial COD had the highest impact on TOC removal efficiency and the "−" sign indicates that this impact is negative; in other words, higher initial COD's resulted in reduced mineralization rates. As for the COD parameter, the second most important process variable was the initial $H_2O_2$ concentration, with a definitely positive effect on TOC removal efficiency, whereas the coefficients of the other two process variables ($Fe^{3+}$ concentration and $t_r$) were found appreciably lower and the relative intensity of their effect on TOC removal is close to each other. Upon compari-

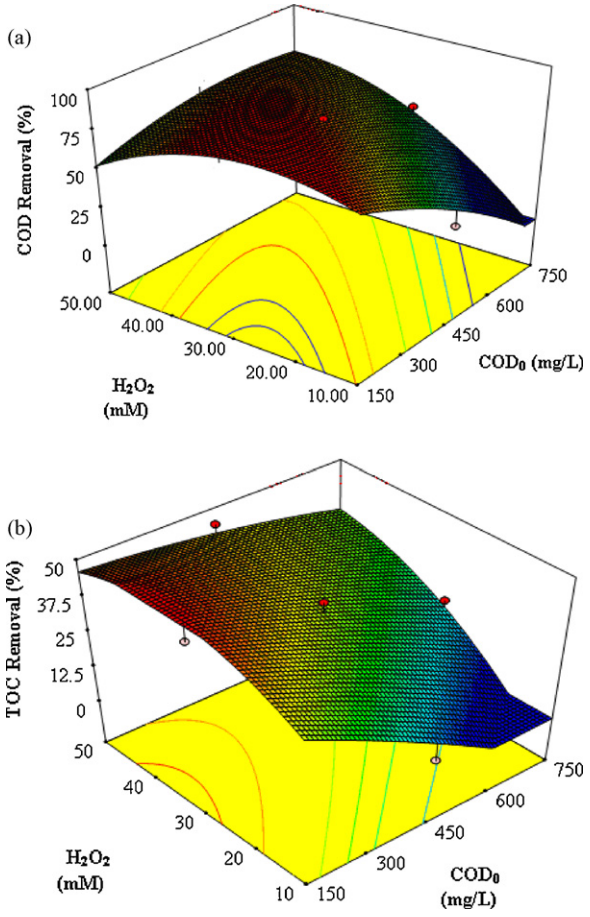


**Fig. 2.** 3D plots for $H_2O_2$–$COD_o$–percent COD (a) and TOC (b) removal efficiency relationships. Experimental conditions: $Fe^{3+}$ = 1.5 mM; $t_r$ = 18 min.

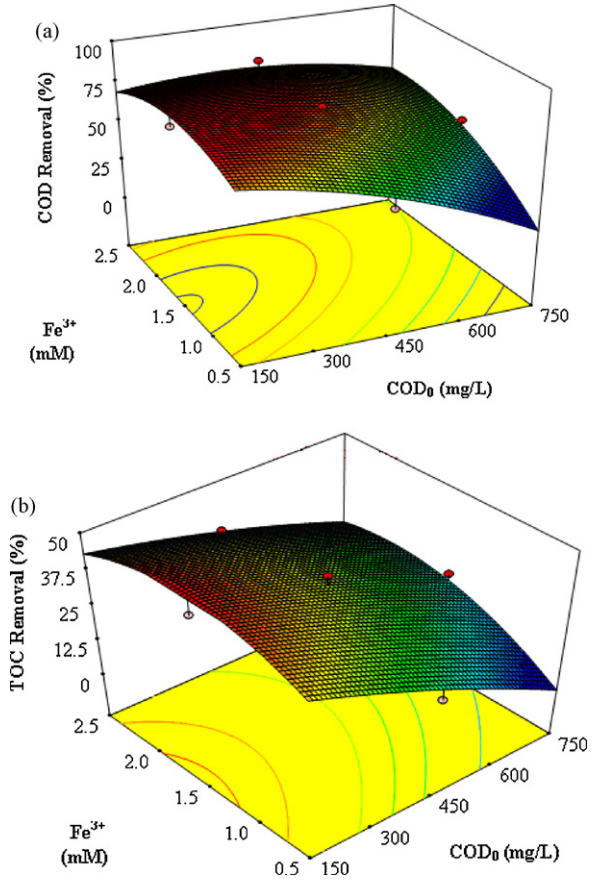


**Fig. 3.** 3D plots for $Fe^{3+}$-$COD_o$-percent COD (a) and TOC (b) removal efficiency relationships. Experimental conditions: $H_2O_2$ = 30 mM; $t_r$ = 18 min.

son of the coefficient values foreseen for the two process dependent variables COD and TOC removal efficiencies it can be deduced that the effects of $COD_o$ and $H_2O_2$ concentration were similar in intensity and orientation, whereas the impact of the process variables $t_r$ and $Fe^{3+}$ concentration were found positive both in terms of COD and TOC removals with considerably higher coefficients found on the basis of TOC removal efficiency. The observation that the coefficients for the process dependent variable TOC are generally speaking higher than for the COD parameter has been evidenced in former related work [36] and can be attributed to the fact that TOC represent ultimate oxidation that is more difficult to achieve than parent compound or COD abatements.

The statistical significance of the established polynomial regression model was evaluated by employing the ANOVA that is a tool offered by the Design Expert® Software to check the adequacy, correctness and fitness of the obtained model equations [45,46]. Table 3 shows ANOVA results found for the quadratic regression model describing the relationship between percent COD and TOC removal efficiencies and the process independent variables selected for Photo-Fenton-like treatment of aqueous H-acid solution. The significance of the proposed model is given by the model *F*- and the probability (Prob > *F*) *F*-values; these were obtained as 8.40 and 0.0006 for COD removal, as well as 8.98 and 0.0004 for TOC removal, respectively. Since a Prob > *F*-value less than 0.0500 is desired for a significant model [47], it is evident that there is only a 0.06% and 0.04% chance that the model is not capable of predicting the experimentally obtained results in terms of COD and TOC removal efficiencies, respectively. The values 0.9145 in terms of COD and 0.9195 in terms of TOC removals obtained for the correlation coefficients ($R^2$) also revealed that the data is fitted well by the polynomial regression models. The adequate precision of the model measures the signal-to-noise ratio and a value of >4 is desirable [47]. The values found for percent COD and TOC removals are both >10 and hence are adequate signals for the model.

### 3.3. Elucidation of relationships between process variables and outputs by 3D plots

For the graphical interpretation of the interactions between process independent variables, the use of 2-and/or 3 dimensional plots of the polynomial regression models is recommended [31,33,34]. These plots are appropriate tools that elucidate the interaction between the four process variables ($COD_o$, $H_2O_2$, $Fe^{3+}$ and $t_r$) and outputs (percent COD and TOC removals) as well as to visualize their combined (interactive) effects. Fig. 2 displays the 3D plots for the $COD_o$–$H_2O_2$–percent COD (a) and $COD_o$–$H_2O_2$–percent TOC (b) removal relationships, whereas Fig. 3 depicts another set of 3-D plots that visualize the interactions between $COD_o$-$Fe^{3+}$-percent COD (a) and $COD_o$-$Fe^{3+}$-percent TOC (b) removals.

From Fig. 2 it is obvious that the applied, initial $H_2O_2$ concentration has a dramatic effect on percent COD and TOC removal efficiencies; this effect is a function of the initial COD content of H-acid solution. For an initial COD of 150 mg/L, an optimum $H_2O_2$ concentration exists to achieve the highest possible COD and TOC removal efficiencies, whereas for $COD_o$ values >150 (based on TOC removal) and 300 (based on COD removal) mg/L, increasing the $H_2O_2$ concentration generally improved the treatment efficiencies. As is apparent from Fig. 2, increasing $COD_o$ resulted in a reduction of TOC removal efficiency in the investigated $COD_o$ range. The

**Table 3**
Presentation of ANOVA results for the established polynomial regression models established for the outputs percent COD and TOC removal.

| | Sum of squares | Degrees of freedom | Mean square | Model *F*-value | Prob > *F* |
|---|---|---|---|---|---|
| COD removal (%) | | | | | |
| Model | 4901.96 | 14 | 350.14 | 8.40 | 0.0006 |
| Residual | 458.43 | 11 | 41.68 | | |
| Lack of Fit | 457.84 | 10 | 45.78 | | |
| Pure Error | 0.59 | 1 | 0.59 | | |
| $R^2$ = 0.9145 | Adequate precision = 10.558 | | | | |
| TOC removal (%) | | | | | |
| Model | 3554.31 | 14 | 253.88 | 8.98 | 0.0004 |
| Residual | 311.16 | 11 | 28.29 | | |
| Lack of Fit | 302.34 | 10 | 30.23 | | |
| Pure Error | 8.82 | 1 | 8.82 | | |
| $R^2$ = 0.9195 | Adequate precision = 10.655 | | | | |

decrease in COD, TOC removal efficiencies is more pronounced at low $H_2O_2$ concentrations (10 and 20 mM $H_2O_2$). On the other hand, COD removal efficiencies were not negatively affected by the initial COD content of the wastewater at $H_2O_2$ concentrations $\geq$30 mM.

From the combinative relationships among $Fe^{3+}$ concentrations, initial COD content and percent COD, TOC removal efficiencies (given in Fig. 3) it is evident that the effect of $Fe^{3+}$ concentration exhibits a similar influence on treatment performance at different initial COD values; however, this influence is not as pronounced as that of initial $H_2O_2$ concentration. This observation is in accordance with the coefficient values obtained for each process variable in the polynomial equations found for COD and TOC removal rates; the coefficients obtained for the variable "$H_2O_2$ concentration" were higher (7.0 in the average) than those found for the variable "$Fe^{3+}$ concentration" (5.0 and 2.5 in Eqs. (6) and (7), respectively).

### 3.4. Validation experiments for Photo-Fenton-like treatment of aqueous H-acid solution

After the polynomial regression models being established to anticipate percent COD and TOC removals for H-acid photocatalytic degradation were analyzed for their statistical significance, the optimum treatment conditions for different initial COD values and their correctness and fitness were questioned for two different targets, namely (i) Photo-Fenton-like treatment conditions required for the achievement of the highest possible oxidation efficiencies in terms of COD and TOC removals; i.e. so-called maximum oxidation-"MO"; (ii) partial oxidation-"PO" at relatively milder reaction conditions that would be sufficient to acquire a specific treatment goal (e.g. a minimum COD level, that is $\leq$200 mg/L) according to the Turkish Water Pollution Control Regulation, required for the discharge of partially treated industrial effluent to receiving water bodies [48]. According to the PO target, COD removal efficiencies have to be specified to satisfy the COD discharge limit value (=200 mg/L effluent COD) and these efficiencies to increase with the increasing initial COD content of aqueous H-acid solution to achieve this limit value. At the same time it was taken into account that due to several operation failures and other routine problems that could be encountered during pretreatment of aqueous H-acid effluent, treatment efficiency might decrease. Hence, it was decided to keep the COD target as 180 mg/L (below 200 mg/L) and set the required percent treatment efficiency accordingly higher, to be on the safe side. Consequently, the established polynomial regression models were fed with the treatment requirements (MO and/or PO) at different initial COD's (local optima) of H-acid solution and a series of validation experiments were run for each initial COD value. It should also be pointed out here that unlike in former studies that questioned only one single Photo-Fenton-like treatment time (the optimum value for the independent process variable $t_r$) indicated for a local ($COD_o$) optima, the validation experiments were confirmed for different reaction times (at least 10 $t_r$ values for each optimum Photo-Fenton-like treatment experiment) during the treatment process. In this way, validation was carried out in a more comprehensive manner and it was possible to confirm whether the models fitted during the whole photocatalytic treatment process. Table 4 indicates the treatment targets (MO; or PO) set for the Photo-Fenton-like oxidation experiments carried out under reaction conditions being optimized based on initial CODs (for $COD_o$ = 150, 300, 450, 600 and 750 mg/L) of aqueous H-acid solutions. As can be followed from Table 4, MO was foreseen at the lower COD's, whereas the target was set as PO for $COD_o$ values >450 mg/L, as well as both MO and PO targets for $COD_o$ values = 450 mg/L.

Table 5 shows experimentally obtained COD and TOC removal efficiencies together with removal rates predicted by the established regression models. In Table 5, results were only shown for the specific optimum $t_r$ value at different $COD_o$ values and treatment performance targets (MO-PO). From Table 5 it is evident that experimentally obtained percent COD and TOC removals were close to the predicted ones for all local optima. It is also obvious from Table 5 that, as expected, the reaction conditions (concentrations and treatment time) foreseen by the factorial design models at local optima are harsher for the target MO than for PO (see conditions given for 450 mg/L $COD_o$-MO and 450 mg/L $COD_o$-PO). Another observation would be that complete oxidation (full oxidation, e.g. mineralization) of H-acid by Photo-Fenton-like treatment was not possible; as was also evident from the preliminary, iterative Photo-Fenton-like experiments, maximum COD and TOC removal efficiencies were found around 80% and 50%, respectively. This could mainly be attributable to the low photonic efficiency of the studied treatment system (on the basis of incident light flux) by employing a UV-A (black light) lamp; it is expected that H-acid competes with ferric iron for the emission band of this near-UV light source. In this manner, effective photoreduction of ferric-hydroxo complexes to ferrous iron will at least partially hindered and the reaction will stops within a short treatment period (e.g. the first 20–25 min of the photocatalytic reaction). The effective photoreduction (recycling) of ferric iron is critical for efficient degradation of target pollutants dominated by the direct, dark Fenton reaction-dominated oxidation mechanism (see Figs. 1 and 5 for experimental results).

Fig. 4 depicts COD and TOC removal efficiencies experimentally obtained during the above mentioned validation experiments as a function of photocatalytic treatment time, together with those removal results predicted by the regression models at the $COD_o$ values 300 mg/L (a) and 600 mg/L (b). The experimental and model results shown in Fig. 4 reveal that the model predictions were satisfactory during the whole Photo-Fenton-like oxidation period and generally within the margins of experimental errors of COD

**Table 4**
Treatment targets (maximum oxidation-MO; partial oxidation-PO) set for the Photo-Fenton-like treatment experiments carried out under reaction conditions being optimized on the basis of different $COD_o$ values of aqueous H-acid solutions.

| $COD_o$ (mg/L)-Target | $Fe^{3+}$ (mM) | $H_2O_2$ (mM) | COD removal (%) | TOC removal (%) |
|---|---|---|---|---|
| 150-MO | In range | In range | Maximize | Maximize |
| 300-MO | In range | In range | Maximize | Maximize |
| 450-PO | In range | In range | 60[a] | Maximize |
| 450-MO | In range | In range | Maximize | Maximize |
| 600-PO | In range | In range | 70[a] | Maximize |
| 750-PO | In range | In range | Maximize[b] | Maximize |

[a] COD removal efficiency target being specified to achieve a final, effluent COD of 180 mg/L according to Turkish discharge consents (COD has to be less than 200 mg/L).
[b] Maximized instead of fixed at a specific COD removal efficiency since otherwise the targeted effluent COD cannot be achieved under the studied reaction conditions.

**Table 5**
Experimentally obtained and predicted treatment efficiencies obtained for the validation experiments conducted under Photo-Fenton-like oxidation conditions being optimized on the basis of initial CODs of aqueous H-acid solution.

| $COD_o$ (mg/L)-Target | $t_r$ (min) | $H_2O_2$ (mM) | $Fe^{3+}$ (mM) | COD removal (%) | | TOC removal (%) | |
|---|---|---|---|---|---|---|---|
| | | | | Model | Experimental | Model | Experimental |
| 150-MO | 23.3 | 30.8 | 1.2 | 84 | 82 ± 8 | 54 | 51 ± 5 |
| 300-MO | 24.0 | 38.1 | 1.6 | 82 | 77 ± 8 | 51 | 44 ± 4 |
| 450-MO | 24.0 | 38.3 | 1.8 | 83 | 79 ± 8 | 46 | 38 ± 4 |
| 450-PO | 12.0 | 40.0 | 1.0 | 64 | 67 ± 7 | 33 | 44 ± 4 |
| 600-PO | 23.9 | 40.0 | 1.1 | 72 | 70 ± 7 | 38 | 41 ± 4 |
| 750-PO | 24.0 | 40.0 | 2.0 | 80 | 76 ± 8 | 35 | 42 ± 4 |

and TOC analyses. Similar accuracies in predicting removal performance as a function of Photo-Fenton-like treatment time were also obtained for the other local optima ($COD_o$ values 150, 450 and 750 mg/L; data not shown).

In addition to the above validation experiments, the correctness and reliability of the obtained regression models was also checked by inserting the experimental data of the preliminary, iterative experiments (see Section 3.1.) in into the polynomial equa-

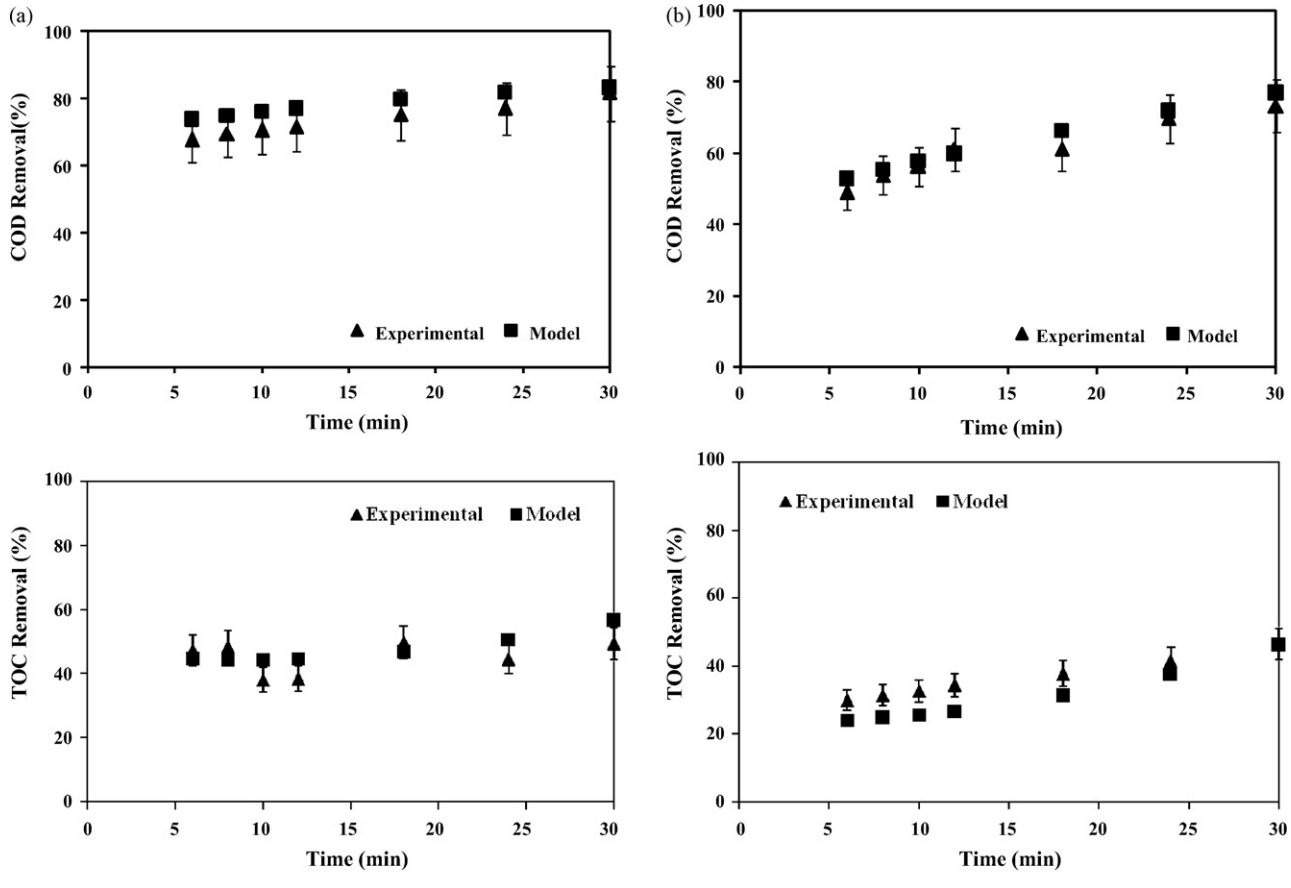


**Fig. 4.** Comparison of changes in experimental and predicted percent COD and TOC removal efficiencies as a function of treatment time obtained during Photo-Fenton-like treatment of aqueous H-acid at $COD_o$ = 300 mg/L under MO conditions (a) and 600 mg/L under PO conditions (b).

tions. Comparison of experimentally obtained and predicted COD and TOC removal efficiencies indicated that the factorial design model was capable of satisfactorily anticipating treatment performances under different photocatalytic reaction conditions (data not shown).

### 3.5. Effect of Photo-Fenton-like treatment on activated sludge inhibition

During the application of AOPs, degradation intermediates being more toxic, inert and/or less biodegradable could be produced [27–29,40]. In order to decide for the most appropriate reaction conditions including treatment time, the effect of photocatalytic degradation products to heterotrophic biomass under Photo-Fenton-like treatment conditions being previously optimized at five different initial COD values (150, 300, 450, 600 and 750 mg/L) of aqueous H-acid solution was also examined. For this purpose, separate activated sludge inhibition experiments were conducted for an incubation period of 30 min with mixed bioculture previously acclimated to synthetic sewage as already described in the Methodology Section (see Section 2.5). Fig. 5 exemplifies $I_{OUR}$ values obtained at H-acid's initial COD values of 300 mg/L (MO), 450(MO) and 750 mg/L (PO) under Photo-Fenton-like oxidation conditions given in Table 5. In Fig. 5, $I_{OUR}$ values are depicted along with changes in parent compound (H-acid), COD and TOC abatements observed during Photo-Fenton-like treatment for the same experimental runs. Although the optimum treatment time was already calculated by the regression models being established for COD and TOC removal efficiencies, percent relative activated sludge inhibition rates (being calculated from the OUR values recorded at an incubation period of 30 min) were determined for different $t_r$ values during the whole Photo-Fenton-like treatment period. From Fig. 5(a) it can be seen that the original H-acid solution not being subjected to photocatalytic treatment exhibits a low inhibitory value of 16% that gradually reduced to 8% at the end of the photocatalytic treatment period. Complete elimination of the inhibitory effect was not observed for any of the experiments speculatively because Photo-Fenton-like treatment never resulted in complete oxidation (mineralization) of H-acid. On the other hand, H-acid was practically entirely degraded within the first 2–5 min. In parallel to H-acid abatement, COD removal slowed down and reached a plateau after 10 min treatment, manifesting that H-acid was converted to some organic intermediates that still exhibited a slight inhibitory effect on the mixed bioculture. At an initial H-acid COD content of 450 mg/L given in Fig. 5(b), PO resulted in parallel H-acid, COD and $I_{OUR}$ abatement; a major reduction occurred within the first 5–10 min of Photo-Fenton-like oxidation, followed by a rather slow abatement period ending with significant, but incomplete oxidation. $I_{OUR}$ values decreased from 11% to only 6% during photocatalytic treatment. The same pattern was observed for Photo-Fenton-like treatment of aqueous H-acid with an initial COD content of 750 mg/L; only slightly lower removal efficiencies and slower abatement rates were achieved at elevated CODs due to the fact that a higher organic carbon content is more difficult to degrade. The inhibitory effect on mixed bioculture dropped down from 18% to 5%. From the above findings it can be concluded that since oxidation was incomplete and TOC removal was limited to not more than 50%, the inhibitory effect could not be completely eliminated, however, no inhibitory/toxic oxidation products were formed throughout the course of Photo-Fenton-like treatment.

In addition, OUR measurements conducted for the same experimental runs given in Fig. 5 could also be regarded as a tool for the assessment of the biodegradability of untreated and photocatalytically treated aqueous H-acid solution [49,50]. OURs obtained after an incubation period of 60 and 90 min steadily increased from 70 to 77 mg/(L h) for $COD_o$ = 300 mg/L after 18 min Photo-Fenton-like treatment; 62 to 72 mg/(L h) for $COD_o$ = 450 mg/L after 24 min Photo-Fenton-like treatment, and 60 to 65 mg/(L h) for $COD_o$ = 750 mg/L after 24 min Photo-Fenton-like treatment, speaking for an average biodegradability improvement of only around 10%.

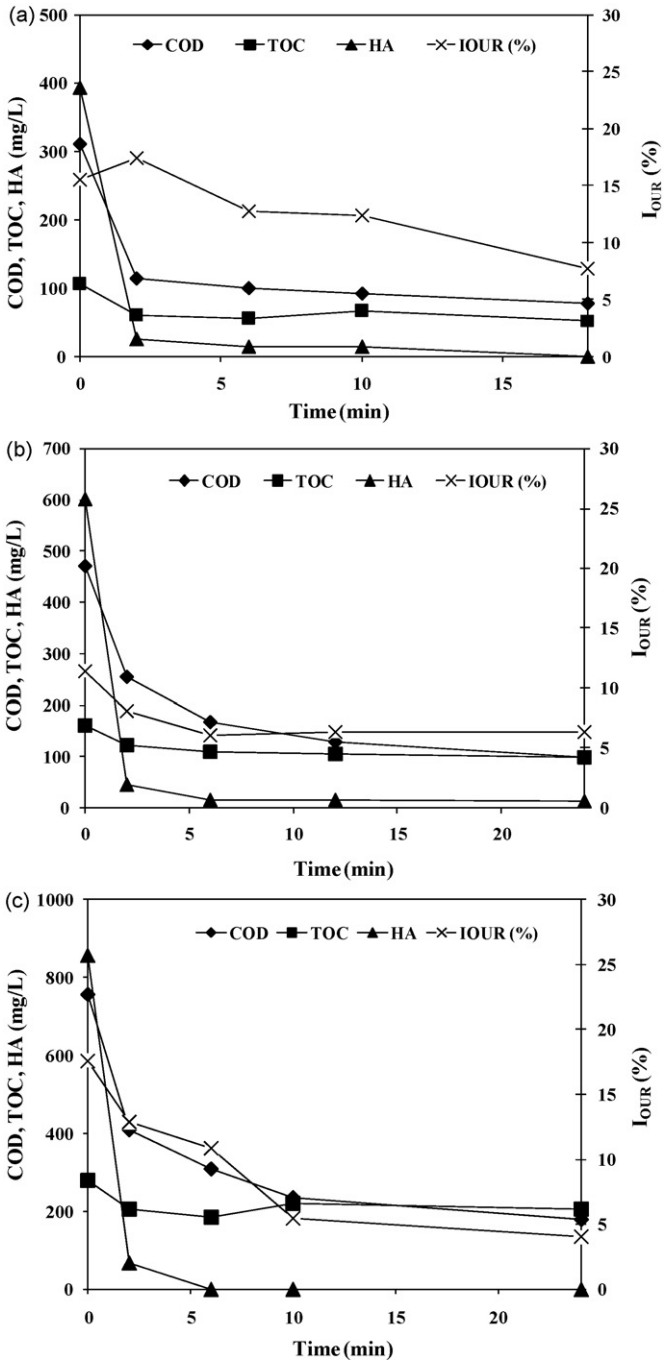


**Fig. 5.** Changes in percent $I_{OUR}$ values in relation with H-acid (abbreviated herein as HA), COD and TOC abatements observed during Photo-Fenton-like treatment of aqueous H-acid at 300 mg/L-MO (a), 450 mg/L-MO (b) and 750 mg/L-PO (c) under optimized reaction conditions. *Experimental conditions*: 1.6 mM $Fe^{3+}$ and 38.1 mM $H_2O_2$ for 300 mg/L $COD_o$; 1.8 mM $Fe^{3+}$ and 38.3 mM $H_2O_2$ for 450 mg/L $COD_o$; 2.0 mM $Fe^{3+}$ and 40.0 mM $H_2O_2$ for 750 mg/L $COD_o$.

## 4. Conclusion and recommendations

An experimental design was applied to empirically model and optimize the Photo-Fenton-like oxidation of the refrac-

tory index pollutant H-acid (1-amino-8-hydroxynaphthalene-3,6-disulphonic acid) in aqueous solution under varying reaction conditions. Experimental results indicated that in particular the process independent variables "initial effluent COD content" and "$H_2O_2$ concentration" played an integral role in the extent of H-acid degradation and mineralization, whereas the parameters "$Fe^{3+}$ concentration" and "reaction time" exhibited relatively minor impacts on the treatment performance under the studied photocatalytic oxidation conditions. Furthermore, once the photocatalytic oxidation process was optimized, complete H-acid removal (achieved within 5–6 min) accompanied with up to 78% oxidation (COD abatement; reached in 20 min) and 65% mineralization (TOC abatement; achieved in 30 min) were obtained. The slightly inhibitory effect of untreated H-acid solution relative to the blank reference (synthetic sewage), decreased to insignificant values (<5%) after application of Photo-Fenton-like oxidation under reaction conditions being optimized with respect to the initial COD contents of aqueous H-acid solutions. From the obtained experimental findings and statistical evaluation of the established regression models it could be deduced that the proposed photocatalytic oxidation system is a kinetically attractive as well as environmentally effective treatment option for originally recalcitrant organic industrial pollutants considering the high treatment efficiencies obtained, the potential of using the UV-A fraction of solar light radiation and working pHs being close to neutral values.

## Acknowledgements

The authors acknowledge the financial support of the Turkish Technical and Scientific Research Council (TUBITAK) under project number 108Y051 and Eksoy Chemicals for the H-acid gift samples.

## References

[1] F.T. Lange, T.P. Knepper, F. Sacher, H.J. Brauch, F. Karrenbrock, O. Roerden, K. Lindner, Waste Manage. 19 (1999) 77–79.
[2] N.C.G. Tan, A. Leeuwen, E.M. Voorthuizen, P. Slenders, Biodegradation 16 (2005) 527–537.
[3] http://www.indiastat.com.
[4] H.S. Freeman, A. Reife, J.S. Gajda, Dyes Pigments 30 (1996) 1–20.
[5] O. Zerbinati, M. Vincenti, S. Pittavino, M.C. Gennaro, Chemosphere 35 (1997) 2295–2305.
[6] P.G. Rieger, H.M. Meier, M. Gerle, U. Vogt, T. Groth, H.J. Knackmuss, J. Biotechnol. 94 (2002) 101–123.
[7] W.H. Glaze, J.W. Kang, D.H. Chapin, Ozone-Sci. Eng. 9 (1987) 335–352.
[8] H. Zhou, D.W. Smith, Can. J. Civil Eng. 28 (2001) 49–66.
[9] T. Oppenländer, Photochemical Purification of Water and Air: Advanced Oxidation Processes (AOPs): Principles, Reaction Mechanisms, Reactor Concepts, Wiley-VCH, Germany, 2003.
[10] V. Calderara, M. Jekel, C. Zaror, Water Sci. Technol. 44 (2001) 7–13.
[11] H. Chen, X. Jin, K. Zhu, R. Yang, Water Res. 36 (2002) 4106–4112.
[12] P. Gehringer, H. Eschweiler, S. Weiss, T. Reemtsma, Ozone-Sci. Eng. 28 (2006) 437–443.
[13] I. Arslan-Alaton, T. Olmez-Hanci, B.H. Gursoy, G. Tureli, Chemosphere 76 (2009) 587–594.
[14] M. Panizza, G. Cerisola, Water Res. 35 (2001) 3987–3992.
[15] K. Swaminathan, S. Sandhya, A.C. Sophia, K. Pachhade, Y.V. Subrahmanyam, Chemosphere 50 (2003) 619–625.
[16] A. Socha, E. Chrzescijanska, E. Kusmierek, Dyes Pigments 67 (2005) 71–75.
[17] A. Socha, E. Chrzescijanska, E. Kusmierek, Dyes Pigments 71 (2006) 10–18.
[18] L. Sun, H. Lu, J. Zhou, Dyes Pigments 76 (2008) 604–609.
[19] G. Yu, W. Zhu, Z. Yang, Z. Li, Chemosphere 36 (1998) 2673–2681.
[20] S. Mohanty, N.N. Rao, P. Khare, S.N. Kaul, Water Res. 39 (2005) 5064–5070.
[21] E. Oliveros, O. Legrini, M. Hohl, T. Müller, A.M. Braun, Chem. Eng. Process. 36 (1997) 397–405.
[22] J.J. Pignatello, Environ. Sci. Technol. 26 (1992) 944–951.
[23] A. Safarzadeh-Amiri, J.R. Bolton, S.R. Cater, J. Adv. Oxid. Technol. 1 (1996) 18–26.
[24] A. Safarzadeh-Amiri, J.R. Bolton, S.R. Cater, Water Res. 31 (1997) 787–798.
[25] P.A. Carneiro, R.F.P. Nogueira, M.V.B. Zanoni, Dyes Pigments 74 (2007) 127–132.
[26] C.A. Emilio, W.F. Jardim, M.I. Litter, H.D. Mansilla, J. Photochem. Photobiol. A 151 (2002) 121–127.
[27] M.J. Farré, S. Brosillon, X. Doménech, J. Peral, J. Photochem. Photobiol. A188 (2007) 34–42.
[28] I. Oller, S. Malato, J.A. Sanchez-Perez, M.I. Maldonado, R. Gasso, Catal. Today 129 (2007) 69–78.
[29] O. Gonzalez, C. Sans, S. Esplugas, J. Hazard. Mater. 146 (2007) 459–464.
[30] R.H. Myers, D.C. Montgomery, Response Surface Methodology: Process and Product Optimization using Designed Experiments, 2nd ed., John Wiley & Sons, New York, 2002.
[31] M. Ahmadi, F. Vahabzadeh, B. Bonakdarpour, E. Mofarrah, M. Mehranian, J. Hazard. Mater. B123 (2005) 187–195.
[32] G. Sudarjanto, B. Keller-Lehmann, J. Keller, J. Hazard. Mater. 138 (2006) 160–168.
[33] A.F. Caliman, C. Cojocaru, A. Antoniadis, I. Poulios, J. Hazard. Mater. 144 (2007) 265–273.
[34] F. Jianfeng, Z. Yaqian, W. Qiuli, J. Hazard. Mater. 144 (2007) 499–505.
[35] C.G. Hatchard, C.A. Parker, Proc. R. Soc. Lond. A235 (1956) 518–536.
[36] I. Arslan-Alaton, G. Tureli, T. Olmez-Hanci, J. Photochem. Photobiol. A 202 (2009) 142–153.
[37] ISO 6060, Water quality-determination of the chemical oxygen demand, ISO 6060/TC 147, 2nd ed., Geneva, 1989.
[38] Official Methods of Analysis, Association of Official Anal. Chemist, Washington, DC, 1980.
[39] ISO 8192, Water quality-oxygen demand inhibition assay by activated sludge, ISO 8192/TC 147/SC 5, Geneva, 2007.
[40] T. Olmez-Hanci, C. Imren, I. Arslan-Alaton, I. Kabdaşlı, O. Tünay, Photochem. Photobiol. Sci. 8 (2009) 620–627.
[41] I. Arslan-Alaton, T. Olmez-Hanci, Z. Kartal, J. Adv. Oxid. Technol. 13 (2010) 27–35.
[42] Eksoy Chemicals, Private communication with technical personnel, Istanbul, 2008.
[43] M. Pérez, F. Torrades, X. Domènech, J. Peral, Water Res. 36 (2002) 2703–2710.
[44] I. Arslan-Alaton, G. Tureli, Fresen. Environ. Bull. 17 (2008) 915–926.
[45] A.F. Martins, C.S. Frank, M.L. Wilde, Clean 35 (2007) 88–99.
[46] B.K. Körbahtı, M.A. Rauf, Chem. Eng. J. 138 (2008) 166–171.
[47] B.K. Körbahtı, M.A. Rauf, J. Hazard. Mater. 161 (2009) 281–286.
[48] The National Water Pollution Control Regulation (WPCR, revised), Official Newspaper, Reference No: 25687, dated December 31, 2004.
[49] H. Spanjers, P.A. Vanrolleghem, Water Sci. Technol. 31 (1995) 105–114.
[50] C.T. Goudar, K.A. Strevett, J. Ind. Microbiol. Biot. 21 (1998) 11–18.